Massive Dirac surface states in topological insulator/magnetic insulator heterostructures

Weidong Luo[1,*] and Xiao-Liang Qi[2,†]

[1]*Geballe Laboratory for Advanced Materials, Stanford University, Stanford, California 94305, USA*

[2]*Department of Physics, Stanford University, Stanford, California 94305, USA*

(Received 2 September 2012; revised manuscript received 5 February 2013; published 19 February 2013)

Topological insulators are new states of matter with a bulk gap and robust gapless surface states protected by time-reversal symmetry. When time-reversal symmetry is broken, the surface states are gapped, which induces a topological response of the system to electromagnetic field—the topological magnetoelectric effect. In this paper we study the behavior of topological surface states in heterostructures formed by a topological insulator and a magnetic insulator. Several magnetic insulators with compatible magnetic structure and relatively good lattice matching with topological insulators Bi_2Se_3, Bi_2Te_3, Sb_2Te_3 are identified, and the best candidate material is found to be MnSe, an antiferromagnetic insulator. We perform first-principles calculations in Bi_2Se_3/MnSe superlattices and obtain the surface state band structure. The magnetic exchange coupling with MnSe induces a gap of ∼54 meV at the surface states. In addition we tune the distance between Mn ions and the topological insulator surface to study the distance dependence of the exchange coupling.

DOI: 10.1103/PhysRevB.87.085431 PACS number(s): 73.20.−r, 85.75.−d

I. INTRODUCTION

Topological insulators (TIs) are new states of quantum matter which have the same symmetry as the conventional insulators and semiconductors but cannot be adiabatically deformed to them without going through a phase transition. Recently, time-reversal invariant (TRI) TIs have been theoretically predicted[1–6] and experimentally realized[7,8] in both two and three dimensions (2D and 3D).[9–11] A TRI TI is characterized by robust surface states and unique, quantized response properties, just like the quantized Hall conductance in 2D quantum Hall states. For 3D TI the topological response is the topological magnetoelectric (TME) effect,[12] which is a magnetoelectric effect with magnetization $\boldsymbol{M}$ generated by electric field $\boldsymbol{E}$ with a quantized coefficient. The TME effect occurs when the surface states of TIs become gapped due to time-reversal symmetry breaking, and is a generic property of 3D topological insulators, which can be obtained theoretically from generic models and from an effective field theory approach,[12,13] independently of microscopic details. Various consequences of the TME effect have been proposed, including Faraday/Kerr rotation of linear polarized light,[12,14–16] the image monopole effect,[17] the charge carried by a magnetic monopole,[18,19] and other types of coupling between the charge and spin degrees of freedom at the TI surface.[20,21] Experimental progress has been made recently on the Faraday/Kerr effect in 3D TI,[22–25] but the quantized effects predicted have not been observed yet.

To realize the TME effect it is essential to introduce time-reversal symmetry breaking (T breaking) at the surface of the TI to make the surface insulating. There are two possible physical ways to open the T-breaking gap at the surface. The first approach is to introduce magnetic impurities such as Mn or Fe to topological insulators. Both the Dirac-type surface states[26] and the bulk states[27] can mediate ferromagnetic coupling between magnetic impurities and thus induce ferromagnetic order under proper conditions. The surface state gap induced by doping magnetic impurities Mn and Fe has been observed in various experiments including transport, angle-resolved photoemission (ARPES), and x-ray magnetic circular dichroism (XMCD).[28–30] This approach has the advantage of a simple experimental setting which can be realized in both bulk materials and thin films. However, the surface state gap is usually small and probably nonuniform due to the low density and disorder effect of the impurities. This may explain why Hall measurements on thin films have observed a large anomalous Hall effect but the longitudinal conductivity is still nonzero.[31] The second approach is to make a heterostructure between a topological insulator and a magnetic insulator (MI), so that the surface states are gapped due to exchange coupling with the MI. Compared to the first approach, this approach has the potential to achieve a stronger and more uniform exchange coupling and thus realize insulating surface states and a TME effect in a higher temperature. The main challenge of this approach is to find the suitable material for the MI, which can form a high-quality heterostructure with topological insulators and lead to a strong exchange coupling. This is the goal of the current work.

In this paper we study heterostructures of the Bi_2Se_3 family of TIs with MIs. We first carried an extensive material search and identified several materials which have relatively the best lattice matching with TIs. The candidate materials are summarized in Table I and their properties will be discussed in more detail in the next section. It is important to notice that some antiferromagnetic insulators can also be used to introduce the surface state gap, although a ferromagnetic exchange coupling at the surface is required. Since the exchange coupling is very short ranged, it will be dominated by the first layer of magnetic ions at the interface of the TI and MI. Therefore if an antiferromagnetic insulator has magnetic moments which are aligned to each other in each layer parallel to the surface, but staggering in the perpendicular direction, it provides the same form of ferromagnetic exchange coupling as a ferromagnetic insulator does. In fact, the best candidate material found in our search is an antiferromagnetic insulator, MnSe, which is a better candidate than ferromagnetic insulators such as EuS since the latter has magnetism from f electrons and has a weaker exchange coupling with the p electrons in TIs

TABLE I. Candidate magnetic insulators and their properties. Here, "L.C." is the lattice constant of the bulk structure, the "lattice matching" is one of the hexagonal 2D crystal planes which should be compared with that of the topological insulators Bi_2Se_3 (4.1355 Å),[32] Bi_2Te_3 (4.395 Å),[33] and Sb_2Te_3 (4.264 Å).[34]

Materials	Structure & L.C.	Lattice matching	Magnetic phase	Comments
EuO	Rock salt, $a = 5.145$ Å	$5.145/\sqrt{2} = 3.64$ Å	FM	$4f$ electrons, weak coupling
EuS	Rock salt, $a = 5.98$ Å	$5.98/\sqrt{2} = 4.23$ Å	FM	$4f$ electrons, weak coupling
EuSe	Rock salt, $a = 6.192$ Å	$6.192/\sqrt{2} = 4.38$ Å	Complex, FM under P	$4f$ electrons, weak coupling
MnSe	Rock salt, $a = 5.464$ Å	$5.464/\sqrt{2} = 3.86$ Å	Type-II AFM, FM (111) planes	$3d$ electrons, stronger coupling
MnTe	Hexagonal, $a = 4.1497$, $c = 6.76$ Å	4.1497 Å	AFM, FM (0001) planes	$3d$ electrons, stronger coupling
$RbMnCl_3$	Hexagonal, $a = 7.16$, $c = 17.83$ Å	$7.16/\sqrt{3} = 4.13$ Å	AFM, FM (0001) planes	Only 1/3 of lattice points

compared with the d electrons in MnSe. We present first-principles calculations in Bi_2Se_3/MnSe superlattices, from which we obtain the surface state gap and also describe it in a surface state effective model. In addition we tune the distance between Mn ions and the TI surface to study the distance dependence of the exchange coupling. Then we conclude by discussing the band-bending effect caused by the interface charge at the TI/MI junction, which is the main experimental challenge that needs to be addressed in future work.

II. CRITERIA AND CANDIDATE MATERIALS

The topological insulators Bi_2Se_3, Bi_2Te_3, and Sb_2Te_3 have layered structures, and the two-dimensional lattice within each layer has a triangular symmetry. The 2D lattice constants of Bi_2Se_3, Bi_2Te_3, and Sb_2Te_3 are 4.1355 Å,[32] 4.395 Å,[33] and 4.264 Å,[34] respectively. We look for candidate MI materials with 2D crystal planes of compatible symmetry to TI layers, i.e., a hexagonal lattice. The other criteria for the candidate MI materials include similar lattice constants and ferromagnetic moments in the 2D hexagonal interface atomic plane.

A list of candidate MI materials is shown in Table I. EuO,[35] EuS,[36] EuSe,[37] and MnSe[38] have the cubic rocksalt structure, of which the atoms in the (111) plane form a triangular lattice, with a lattice constant compatible with the TIs. Both EuO and EuS are ferromagnetic insulators, which meets the requirement of correct magnetic configuration; however, the lattice constant of EuO is too small for good lattice matching with the common 3D topological insulators. EuSe has a complex magnetic phase diagram, and it also becomes FM under suitable pressure range. Magnetism in EuO, EuS, and EuSe originates from the half-filled $4f$ orbitals of the Eu^{+2} ions. MnSe has the type-II (G-type) antiferromagnetic (AFM) structure, of which the magnetic moments in each (111) atomic planes are ferromagnetic. MnTe[39] is chemically similar to MnSe, although it has a hexagonal lattice. Mn moments in MnTe also have an AFM configuration, formed of alternating hexagonal (0001) FM planes. Magnetism in MnSe and MnTe originates from the high-spin d^5 orbitals of the Mn^{+2} ions. $RbMnCl_3$ is also in a hexagonal structure,[40] with the Mn sites forming alternating (0001) FM planes. Although its hexagonal plane has a much larger lattice constant, it matches the $\sqrt{3} \times \sqrt{3}$ reconstruction of the in-plane lattice of Bi_2Se_3. Thus $RbMnCl_3$ is a potential candidate material, although the magnetic coupling would be weaker because only 1/3 of the atomic sites of the TIs will be in contact with the Mn sites.

In the candidate materials listed in Table I, we performed first-principles calculations on several of them including Bi_2Se_3/MnSe, Sb_2Te_3/MnTe, and Bi_2Se_3/MnTe. Among these heterostructures, we find Bi_2Se_3/MnSe to be the best one, with relatively strong exchange coupling and simple surface state band structure. In the following we will focus on the results of Bi_2Se_3/MnSe heterostructure, and present the results on Sb_2Te_3/MnTe and Bi_2Se_3/MnTe as a comparison.

III. Bi_2Se_3/MnSe INTERFACE

We study the Bi_2Se_3/MnSe interface by constructing a superlattice composed of Bi_2Se_3 and MnSe slabs. The supercells employed in the first-principles calculations are required to have inversion symmetry, and the Mn atoms at the top and bottom surfaces of the Bi_2Se_3 slab have parallel spin orientation. The thickness of the Bi_2Se_3 slab is chosen to be four quintuple layers (QLs), the MnSe slab is determined to have a thickness of $6n + 1$ (7, 13, 19, ...) layers, in order to meet the requirements of inversion symmetry and parallel spin orientations. To simulate the physical system of a MnSe film deposited on top of a bulk Bi_2Se_3, the in-plane lattice constant of the MnSe is fixed to that of Bi_2Se_3, and the out-of-plane lattice constant is determined by energy optimization. The 4-7 supercell structure (composed of four QLs of Bi_2Se_3 and seven layers of MnSe) is shown in Fig. 1(b).

First-principles density functional theory (DFT) calculations are performed to optimize the supercell structure and to obtain the electronic band structure. We used

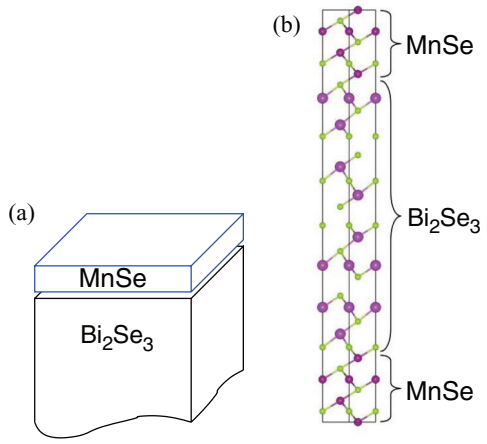

FIG. 1. (Color online) (a) Schematic picture of a MnSe film deposited on the surface of Bi_2Se_3. (b) Crystal structure of the supercell structure in the first-principles calculations.

the Hohenberg-Kohn DFT with the generalized-gradient approximation (GGA)[41] and the projector augmented-wave method as implemented in VASP.[42–44] The Mn $3d$ orbitals are treated with the GGA plus Hubbard U (GGA + U) method,[45,46] and typical values of correlation parameters are used:[47,48] $U = 5.0$ eV, and $J = 1.0$ eV.

We would like to describe the experimental setting of a magnetic insulator film grown on top of a topological insulator substrate, in which case we expect the in-plane lattice constant of the MI is matched to the TI, while the out-of-plane lattice constant of the MI is relaxed. If not noted otherwise (as when tuning the separation distance between Bi_2Se_3 and MnSe slabs), the atomic coordinates of the superlattice in the calculations are optimized as in the following. The middle part of the Bi_2Se_3 slab is fixed to the experimental structure, while the atomic coordinates of the whole MnSe slab together with the first Bi and Se atomic planes at both surfaces of the Bi_2Se_3 slab are optimized according to the forces from first-principles calculations.

A. Band structure

We first investigate the 4-13 Bi_2Se_3/MnSe superlattice, with Mn spins along [001] direction. The band structure from first-principles calculations is shown in Fig. 2. By projecting the bands to the Bi and Se atoms of the top and bottom surfaces, shown in Fig. 2(a), we identify the Dirac cone feature located about 0.4 eV below the bulk gap of Bi_2Se_3 as surface states of Bi_2Se_3. Further analysis on the spin directions of the states around the Γ point confirms it to be the topological surface state. A small gap appears at the Dirac point, and both the lower and upper Dirac cones show spin-related energy splitting in the vicinity of Γ point, indicating a gap opening due to magnetic interaction with MnSe.

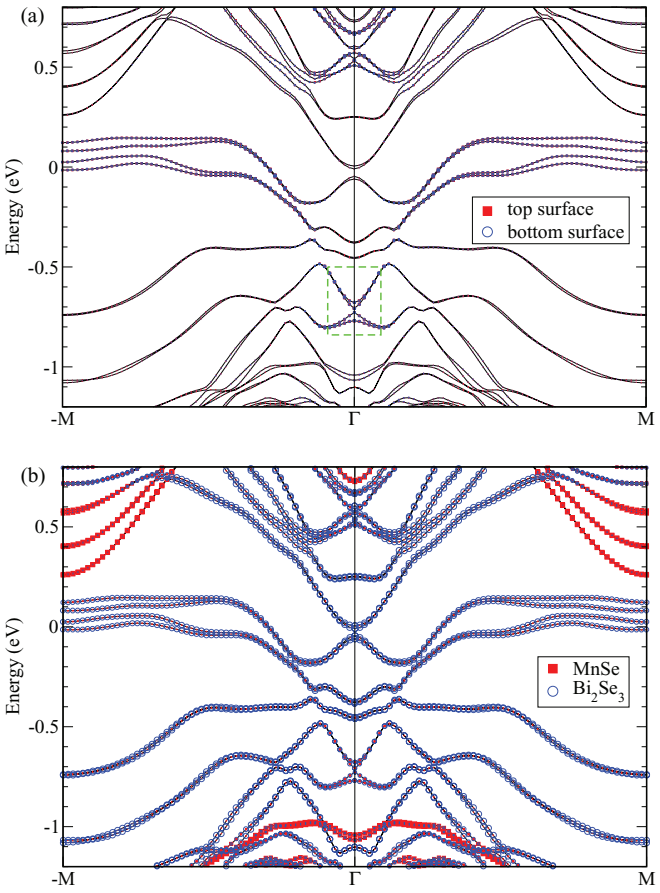

FIG. 2. (Color online) Band structure of the Bi_2Se_3/MnSe superlattice. The two panels show the projection of the wave functions to the Bi and Se atoms at the top and bottom surfaces (a), and that to the two materials Bi_2Se_3 and MnSe (b). The calculation is done for the superlattice structure composed of four quintuple layers of Bi_2Se_3 and 13 layers of MnSe, with Mn spins along [001] direction.

The band gap of MnSe is much larger than that of Bi_2Se_3. To obtain a clearer picture of the electronic states of the two materials forming the superlattice, we project the bands separately to the Bi_2Se_3 slab and to the MnSe slab, shown in Fig. 2(b). The bulk gap of Bi_2Se_3, as well as the Dirac cone states, are located in the band gap of MnSe, which makes it possible to realize a fully gapped system and observe the TME effect.

B. Effective model fitting

To gain better understanding of the exchange coupling experienced by the surface states, we introduce an effective Hamiltonian H_{eff} for the Dirac fermion surface states of the topological insulator thin film coupled with the exchange field[49]

$$H_{\text{eff}} = Dk^2 I + \begin{pmatrix} \hbar v_F(\sigma_x k_y - \sigma_y k_x) + \boldsymbol{M}\cdot\boldsymbol{\sigma} & tI \\ tI & -\hbar v_F(\sigma_x k_y - \sigma_y k_x) + \boldsymbol{M}\cdot\boldsymbol{\sigma} \end{pmatrix}, \quad (1)$$

Here σ_i $(i = x,y,z)$ are the Pauli matrices, and I the identity matrix. $\boldsymbol{M}$ and t correspond to the effective magnetic field acting on the Dirac fermion surface states and the inter-edge interaction between the two surfaces. The other parameters in the model are D the quadratic term, and v_F the Fermi velocity.

The eigenenergies of the model Hamiltonian can be solved analytically,

$$E = Dk^2 \pm \sqrt{k^2 + M^2 + t^2 \pm 2\sqrt{M^2t^2 + (M_xk_y - M_yk_x)^2}}, \quad (2)$$

here we set $\hbar v_F = 1$. We note that at the Γ point ($k = 0$), the four eigenenergies are $E = \pm(M \pm t)$. In the case of strong magnetic coupling and weak inter-edge interaction when $M > t$, the zone-center eigenenergies (from low energy to high energy) and the corresponding spin orientations are $-M - t$ (spin down), $-M + t$ (spin down), $M - t$ (spin up), and $M + t$ (spin up). In the opposite case when $M < t$, the zone-center eigenenergies and spin orientations are $-M - t$ (spin down), $M - t$ (spin up), $-M + t$ (spin down), and $M + t$ (spin up). In both cases, an energy gap Δ forms at the original Dirac point, $\Delta = 2|M - t|$.

The Dirac fermion band structure obtained from first-principles calculations is fitted to the model solution in Eq. (2). For the superlattice structure composed of four quintuple layers of Bi_2Se_3 and 13 layers of MnSe with Mn spins along [001] direction, the calculated Dirac fermion surface states around the Γ point are fitted satisfactorily to the model solution, as shown in Fig. 3(a) for crystal momentum along the k_x (Γ-M) direction. The fitting parameters are $M = 28.2$ meV, $t = 17.6$ meV, $D = 9.8$ eV Å^2, and $v_F = 2.66\times10^5$ m/s. Fitting the model solution to the calculated band dispersion along the k_y (Γ-K) direction gives very similar parameters, $D = 9.9$ eV Å^2, and $v_F = 2.70\times10^5$ m/s. It should be noticed that our fitting yields a smaller v_F than a previous theoretical value[50] because our fitting is done for a finite range of momentum so that the quadratic term plays an important role. We also note that our v_F value agrees well with recent experimental measurements[51,52] of $v_F \sim 3.3\times10^5$ m/s.

C. Distance dependence of parameters t and M

To understand the behavior of a large physical system, we investigate the dependence of the effective magnetic field M and inter-edge interaction t on the thickness of the MnSe slab in the superlattice. First-principles band structure calculations on the 4-7 (composed of four QLs of Bi_2Se_3 and seven layers of MnSe), 4-13, and 4-19 Bi_2Se_3/MnSe superlattices were fitted to the model solution using Eq. (2). The fitting parameters M and t are plotted as a function of the MnSe layer number, as shown in Fig. 3(b). The effective magnetic field M does not vary strongly as the number of MnSe layers increases, consistent with the fact that it is mostly due to the magnetic exchange coupling between the interface MnSe and the surface states of Bi_2Se_3. In contrast, the inter-edge interaction t decreases rapidly as the number of MnSe layers increases. This indicates that the inter-edge interaction in smaller superlattices are mediated mostly through the MnSe slab, instead of within the Bi_2Se_3 layers. This result is consistent with previous study of free-standing Bi_2Se_3 films, which shows that the inter-edge coupling is already very small for four QLs.[53] The strong effective magnetic field ($M \sim 27$ meV) at this interface results in a large gap opening ($2M \sim 54$ meV) in a realistic experimental setup with a thicker MnSe slab where $t \sim 0$, which holds promise for magnetic manipulation of TI surface states at room temperature.

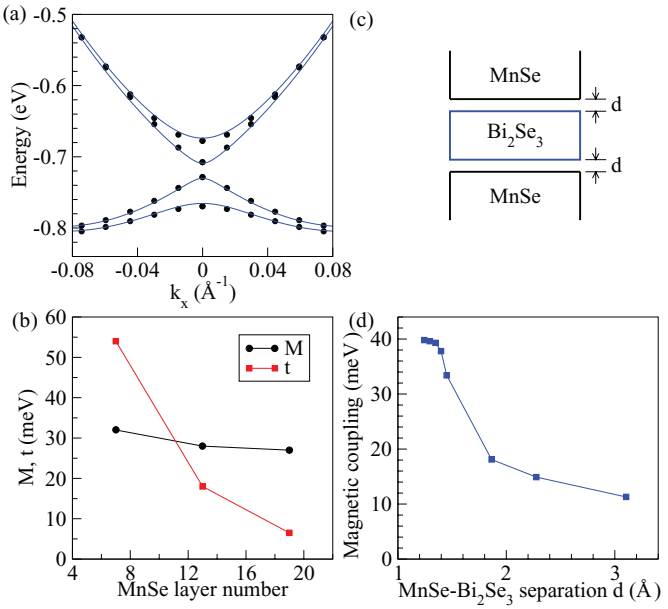

FIG. 3. (Color online) (a) The calculated band structure (black circle, the same data as in Fig. 2) is fitted by the effective model (1) (blue curves). (b) The dependence of the inter-edge interaction t and the effective exchange field M on the thickness of the MnSe slab, obtained from the fitting. (c) A schematic picture of the material structure used in the calculations shown in (d), with the distance d between MnSe and Bi_2Se_3 tuned (see text). (d) Dependence of M on the separation d between the Bi_2Se_3 and MnSe slabs. For comparison, the layer separation d between Bi_2Se_3 and MnSe of the relaxed structure is 1.45 Å.

In our calculations a perfect interface between MnSe and Bi_2Se_3 is assumed. In reality, the interface will probably contain impurities and defects, so the coupling between Mn and Se across the interface is weaker. To see how the magnetic exchange coupling is affected by the distance between Mn and Se atoms, we now keep fixed the atomic coordinates within the Bi_2Se_3 and MnSe slabs, but we vary the separation d between the Bi_2Se_3 and MnSe slabs, as shown in Fig. 3(c). Because the effective magnetic field M is mostly due to the exchange coupling between MnSe and Bi_2Se_3 across the interface, we expect a strong dependence of M on the separation distance d. For the 4-13 Bi_2Se_3/MnSe superlattice, the effective magnetic field M is plotted in Fig. 3(d), showing a strong dependence of M as a function of the separation between Bi_2Se_3 and MnSe. This result indicates that the magnetic exchange coupling at the TI-MI interface could be tuned by applying external pressure.

D. Surface charge and band bending

Although the Dirac cone is in the bulk gap of MnSe, from the band structure shown in Fig. 2 we see some additional hole-type bands coexisting with the massive Dirac cone.

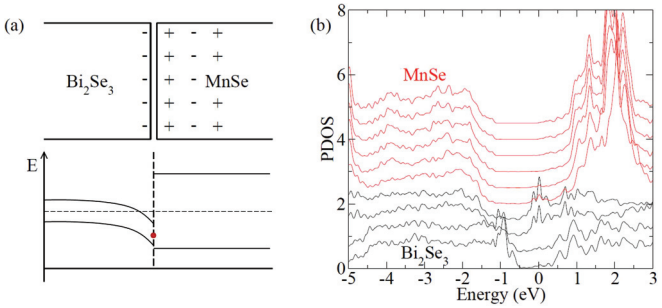

FIG. 4. (Color online) (a) Charge states at the Bi_2Se_3/MnSe interface, and a schematic picture of band bending, where the (red) dot at the interface represents the surface state Dirac point. (b) The calculated projected density-of-states of Bi_2Se_3 (black) and MnSe (red) lattice planes at the interface, showing the band bending. Here each curve for MnSe represents one Mn-Se bilayer, and each curve for Bi_2Se_3 represents one Bi-Se bilayer in either the top or bottom half of the quintuple layers.

These bands can be understood as a consequence of the band bending occurring at the interface. Band bending at a heterojunction is common. In MnSe, Mn^{2+} and Se^{2-} ions carry a positive and negative charge, respectively. Consequently, the Mn terminated surface considered here carries a finite positive charge density. Since the Bi_2Se_3 is a covalent material and has no surface charge, the net charge of the interface between these two materials is positive, leading to a trap for the surface electrons. Therefore the bands bend down around the interface, as illustrated in Fig. 4(a), leading to the additional surface state bands.

We studied the band bending effect by calculating the electronic density-of-states projected to individual lattice planes around the interface. The projected density-of-states (PDOS) of the Mn-Se atomic bilayers are shown in red curves in Fig. 4(b), while the PDOS of the Bi-Se atomic bilayers in the top and bottom halves of the Bi_2Se_3 quintuple layers are shown in black curves. It is clear that very little band bending exists in MnSe, while there is significant energy shift between the first and the second QLs of Bi_2Se_3. The electronic states in the first QL of Bi_2Se_3 is shifted down in energy compared to the second QL, consistent with the direction of the interface electric dipole moment shown in Fig. 4(a).

The additional surface states make the surface metallic and lead to difficulty in achieving an insulating surface. In principle the additional surface states will always be localized by the disorder effect at low temperature since there is no topological protection, and time-reversal symmetry is broken. However, it is very possible that the localization temperature is very low, so that in experimental temperatures the additional surface states may still be metallic. The solution of this problem is the main open question we leave for future theoretical and experimental work. Possible solutions include screening the surface charge by a top gate, or by proper chemical doping at the junction. We would like to note that the consequences of the TME effect, such as the image monopole effect,[17] can still be observed in the presence of the metallic surface states with a modified experimental setting.[54]

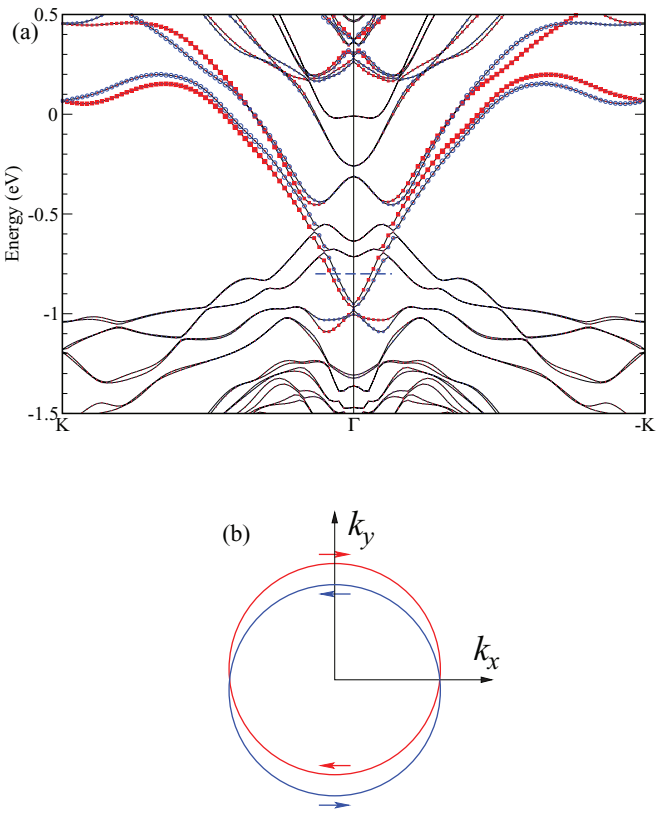

FIG. 5. (Color online) In-plane magnetization. (a) Band structure of the Bi_2Se_3/MnSe superlattice along the k_y (Γ-K) direction. The red and blue symbols show the projection of the wave functions to the Bi and Se atoms at the top and the bottom surfaces. (b) A schematic showing the Fermi surfaces of n-doped surface states at the two surfaces of Bi_2Se_3. The Fermi energy is taken at the dashed line in (a). The calculation is performed for superlattice structure composed of four QLs of Bi_2Se_3 and 13 layers of MnSe, with Mn spins along the in-plane [100] direction.

E. In-plane magnetization

As a comparison, we also calculated the band structure of the Bi_2Se_3/MnSe superlattice with Mn spins along the in-plane [100] direction. The band structure along the k_y (Γ-K) direction with projection of the bands to the Bi and Se atoms of the top and bottom surfaces is shown in Fig. 5(a). Similar to the case of [001] spin orientation shown in Fig. 2, the Dirac-cone states are located about 0.4 eV below the bulk gap of Bi_2Se_3. One prominent feature is that the Dirac-cone states of the top and bottom surfaces are shifted to opposite directions along the k_y axis. For a Fermi energy above the Dirac cone, the Fermi surfaces from the top and bottom surfaces of Bi_2Se_3 will shift to opposite directions in the momentum space. Figure 5(b) illustrates the opposite shift of the two Fermi surfaces along the k_y direction, and the corresponding spin directions.

By fitting the effective model solution [Eq. (2)] with an in-plane exchange field, we extracted the exchange coupling M and inter-edge interaction t. For the 4-13 superlattice structure with in-plane magnetization, we obtain $M = 9$ meV and $t = 19$ meV. The value of t mostly depends on the thickness of MnSe and Bi_2Se_3 slabs, so t in the case of in-plane magnetization is similar to the value for perpendicular

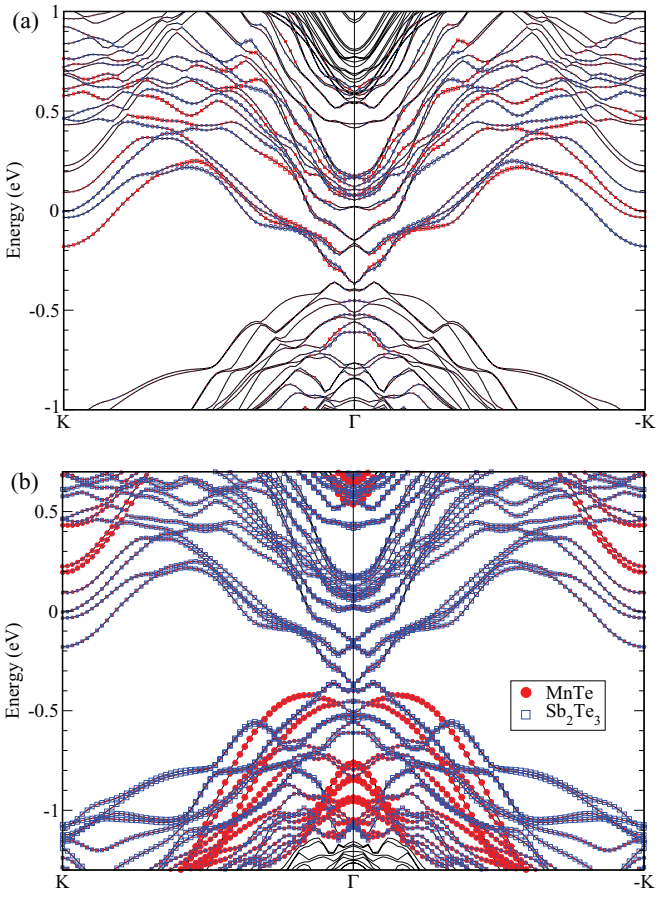

FIG. 6. (Color online) Band structure of the Sb_2Te_3/MnTe superlattice. The two panels show the projection of the wave functions to the Sb and Te atoms at the top (red symbols) and the bottom (blue symbols) surfaces (a), and that to the two materials Sb_2Te_3 and MnTe (b). The calculation is done for the superlattice structure composed of four QLs of Sb_2Te_3 and 13 layers of MnTe, with Mn spins along the [001] direction.

magnetization. However, the exchange coupling is quite anisotropic, and it is much smaller in the case of in-plane magnetization compared to the perpendicular one.

IV. OTHER CANDIDATE MATERIALS

Other materials in our study include the Sb_2Te_3/MnTe and Bi_2Se_3/MnTe heterostructures. The calculated band structure of the 4-13 superlattice with projection of the bands to the Sb and Te atoms at the top and bottom surfaces is shown in Fig. 6(a). In contrast to the Bi_2Se_3/MnSe heterostructure, there is complicated hybridization of bulk and surface states in the Sb_2Te_3/MnTe heterostructure, and the Dirac-cone feature cannot be easily identified.

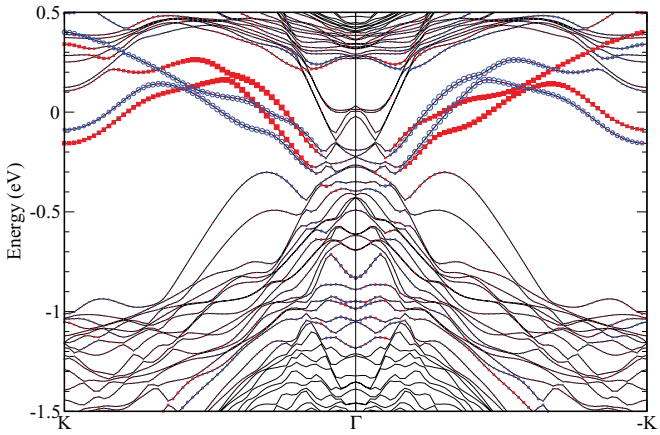

FIG. 7. (Color online) Band structure of the Bi_2Se_3/MnTe superlattice, showing the projection of the wave functions to the Bi and Se atoms at the top (red symbols) and the bottom (blue symbols) surfaces. The calculation is done for the superlattice structure composed of four QLs of Bi_2Se_3 and seven layers of MnTe, with Mn spins along the [001] direction.

We project the bands separately to the Sb_2Te_3 slab and the MnTe slab in the superlattice, as shown in Fig. 6(b). Although the bulk band gap of MnTe at the Γ point is much larger than Sb_2Te_3, the bulk band gap of Sb_2Te_3 is located close in energy to the top of the valence band of MnTe, and the Dirac surface states overlap in energy with the valence band of MnTe. Therefore it is less likely to realize a fully gapped system in the Sb_2Te_3/MnTe heterostructure.

We have also studied the Bi_2Se_3/MnTe heterostructure with a supercell composed of four QLs of Bi_2Se_3 and seven layers of MnTe. The calculated band structure with projection of the bands to the Bi and Se atoms at the top and bottom surfaces is shown in Fig. 7. Similar to the Sb_2Te_3/MnTe heterostructure, the surface states and bulk states in the Bi_2Se_3/MnTe heterostructure are also strongly hybridized, and the Dirac-cone feature cannot be easily identified.

ACKNOWLEDGMENTS

We acknowledge helpful discussions with Haijun Zhang and Shou-Cheng Zhang. This work is supported by the Defense Advanced Research Projects Agency Microsystems Technology Office, MesoDynamic Architecture Program (MESO) through Contract No. N66001-11-1-4105. Computations were performed at the National Energy Research Scientific Computing Center, which is supported by the Office of Science of the U.S. Department of Energy under Contract No. DE-AC02-05CH11231.

*Present address: Department of Physics and Institute of Natural Sciences, Shanghai Jiao Tong University, Shanghai 200240, China; wdluo@sjtu.edu.cn

†xlqi@stanford.edu

[1] C. L. Kane and E. J. Mele, Phys. Rev. Lett. **95**, 226801 (2005).

[2] B. A. Bernevig and S. C. Zhang, Phys. Rev. Lett. **96**, 106802 (2006).

[3]B. A. Bernevig, T. L. Hughes, and S. C. Zhang, Science **314**, 1757 (2006).
[4]R. Roy, Phys. Rev. B **79**, 195322 (2009).
[5]J. E. Moore and L. Balents, Phys. Rev. B **75**, 121306 (2007).
[6]L. Fu, C. L. Kane, and E. J. Mele, Phys. Rev. Lett. **98**, 106803 (2007).
[7]M. König, S. Wiedmann, C. Brüne, A. Roth, H. Buhmann, L. Molenkamp, X.-L. Qi, and S.-C. Zhang, Science **318**, 766 (2007).
[8]D. Hsieh, D. Qian, L. Wray, Y. Xia, Y. S. Hor, R. J. Cava, and M. Z. Hasan, Nature **452**, 970 (2008).
[9]J. E. Moore, Nature **464**, 194 (2010).
[10]M. Z. Hasan and C. L. Kane, Rev. Mod. Phys. **82**, 3045 (2010).
[11]X.-L. Qi and S.-C. Zhang, Rev. Mod. Phys. **83**, 1057 (2011).
[12]X.-L. Qi, T. L. Hughes, and S.-C. Zhang, Phys. Rev. B **78**, 195424 (2008).
[13]A. M. Essin, J. E. Moore, and D. Vanderbilt, Phys. Rev. Lett. **102**, 146805 (2009).
[14]A. Karch, Phys. Rev. Lett. **103**, 171601 (2009).
[15]J. Maciejko, X.-L. Qi, H. D. Drew, and S.-C. Zhang, Phys. Rev. Lett. **105**, 166803 (2010).
[16]W.-K. Tse and A. H. MacDonald, Phys. Rev. Lett. **105**, 057401 (2010).
[17]X.-L. Qi, R. Li, J. Zang, and S.-C. Zhang, Science **323**, 1184 (2009).
[18]G. Rosenberg and M. Franz, Phys. Rev. B **82**, 035105 (2010).
[19]G. Rosenberg, H.-M. Guo, and M. Franz, Phys. Rev. B **82**, 041104 (2010).
[20]T. Yokoyama, J. Zang, and N. Nagaosa, Phys. Rev. B **81**, 241410 (2010).
[21]K. Nomura and N. Nagaosa, Phys. Rev. B **82**, 161401(R) (2010).
[22]R. V. Aguilar, A. Stier, W. Liu, L. Bilbro, D. George, N. Bansal, J. Cerne, A. Markelz, S. Oh, and N. Armitage, arXiv:1105.0237.
[23]A. D. LaForge, A. Frenzel, B. C. Pursley, T. Lin, X. Liu, J. Shi, and D. N. Basov, Phys. Rev. B **81**, 125120 (2010).
[24]A. B. Sushkov, G. S. Jenkins, D. C. Schmadel, N. P. Butch, J. Paglione, and H. D. Drew, Phys. Rev. B **82**, 125110 (2010).
[25]G. S. Jenkins, A. B. Sushkov, D. C. Schmadel, N. P. Butch, P. Syers, J. Paglione, and H. D. Drew, Phys. Rev. B **82**, 125120 (2010).
[26]Q. Liu, C.-X. Liu, C. Xu, X.-L. Qi, and S.-C. Zhang, Phys. Rev. Lett. **102**, 156603 (2009).
[27]R. Yu, W. Zhang, H. J. Zhang, S. C. Zhang, X. Dai, and Z. Fang, Science **329**, 61 (2010).
[28]Y. L. Chen, J.-H. Chu, J. G. Analytis, Z. K. Liu, K. Igarashi, H.-H. Kuo, X. L. Qi, S. K. Mo, R. G. Moore, D. H. Lu, M. Hashimoto, T. Sasagawa, S. C. Zhang, I. R. Fisher, Z. Hussain, and Z. X. Shen, Science **329**, 659 (2010).
[29]S.-Y. Xu, M. Neupane, C. Liu, D. M. Zhang, A. Richardella, L. A. Wray, N. Alidoust, M. Leandersson, T. Balasubramanian, J. Sachez-Barriga, O. Rader, G. Landolt, B. Slomski, J. H. Dil, T.-R. Chang, J. Osterwalder, H.-T. Jeng, H. Lin, A. Bansil, N. Samarth, and M. Z. Hasan, arXiv:1206.2090.
[30]M. Liu, J. Zhang, C.-Z. Chang, Z. Zhang, X. Feng, K. Li, K. He, L.-l. Wang, X. Chen, X. Dai, Z. Fang, Q.-K. Xue, X. Ma, and Y. Wang, Phys. Rev. Lett. **108**, 036805 (2012).
[31]C.-Z. Chang, J.-S. Zhang, M.-H. Liu, Z.-C. Zhang, X. Feng, K. Li, L.-L. Wang, X. Chen, X. Dai, Z. Fang, X.-L. Qi, S.-C. Zhang, Y. Wang, K. He, X.-C. Ma, and Q.-K. Xue, arXiv:1108.4754.
[32]C. Pérez Vicente, J. L. Tirado, K. Adouby, J. C. Jumas, A. Abba Touré, and G. Kra, Inorg. Chem. **38**, 2131 (1999).
[33]Y. Feutelais, B. Legendre, N. Rodier, and V. Agafonov, Mater. Res. Bull. **28**, 591 (1993).
[34]T. L. Anderson and H. B. Krause, Acta Crystallogr. B **30**, 1307 (1974).
[35]D. B. McWhan, P. C. Souers, and G. Jura, Phys. Rev. **143**, 385 (1966).
[36]M. Palazii and E. Bretey, Mater. Res. Bull. **24**, 695 (1989).
[37]K. Westerholt and H. Bach, Phys. Rev. B **31**, 7151 (1985).
[38]A. J. Jacobson and B. E. F. Fender, J. Chem. Phys. **52**, 4563 (1970).
[39]S. S. A. Noor, J. Appl. Phys. **61**, 3549 (1987).
[40]E. M. Ali and A. A. Felimban, Aust. J. Phys. **42**, 307 (1989).
[41]J. P. Perdew, K. Burke, and M. Ernzerhof, Phys. Rev. Lett. **77**, 3865 (1996).
[42]P. E. Blöchl, Phys. Rev. B **50**, 17953 (1994).
[43]G. Kresse and J. Furthmüller, Phys. Rev. B **54**, 11169 (1996).
[44]G. Kresse and D. Joubert, Phys. Rev. B **59**, 1758 (1999).
[45]V. I. Anisimov, J. Zaanen, and O. K. Andersen, Phys. Rev. B **44**, 943 (1991).
[46]A. I. Liechtenstein, V. I. Anisimov, and J. Zaanen, Phys. Rev. B **52**, R5467 (1995).
[47]S. J. Youn, J. Magnetics **10**, 71 (2005).
[48]P. Amiri, S. J. Hashemifar, and H. Akbarzadeh, Phys. Rev. B **83**, 165424 (2011).
[49]C.-X. Liu, X.-L. Qi, H. J. Zhang, X. Dai, Z. Fang, and S.-C. Zhang, Phys. Rev. B **82**, 045122 (2010).
[50]H. Zhang, C.-X. Liu, X.-L. Qi, X. Dai, Z. Fang, and S.-C. Zhang, Nat. Phys. **5**, 438 (2009).
[51]P. Cheng, C. Song, T. Zhang, Y. Zhang, Y. Wang, J.-F. Jia, J. Wang, Y. Wang, B.-F. Zhu, X. Chen, X. Ma, K. He, L. Wang, X. Dai, Z. Fang, X. C. Xie, X.-L. Qi, C.-X. Liu, S.-C. Zhang, and Q.-K. Xue, Phys. Rev. Lett. **105**, 076801 (2010).
[52]A. A. Taskin, S. Sasaki, K. Segawa, and Y. Ando, Phys. Rev. Lett. **109**, 066803 (2012).
[53]C.-X. Liu, H. J. Zhang, B. Yan, X.-L. Qi, T. Frauenheim, X. Dai, Z. Fang, and S.-C. Zhang, Phys. Rev. B **81**, 041307(R) (2010).
[54]D. A. Pesin and A. H. MacDonald, arXiv:1207.4444.